JOURNAL OF AIRCRAFT
Vol. 37, No. 3, May–June 2000

Characteristics of Transonic Rectangular Cavity Flows

Kung-Ming Chung*
National Cheng-Kung University, Tainan 711, Taiwan, Republic of China

Experiments are performed to study the characteristics of rectangular cavity flows. Mean and fluctuating surface pressure in a Mach-1.28 turbulent flow past rectangular cavities are obtained. The cavity length-to-depth ratio *L/D* varies from 2.43 to 43.00, and the length-to-width ratio *L/W* is 0.5, 1.0, and 2.0. The effect of cavity depth is studied, in which *L/W* or both *L/D* and *L/W* are held constant. The results indicate that *L/D* is the most important parameter in determining the characteristics inside the cavity and in its vicinity. The effect of *L/W* is significant only at the aft half of the cavity. Lower static pressure aft of the front face and higher static pressure at the aft half of the cavity are observed with decreasing depth-to-incoming boundary-layer thickness D/δ_0 at constant *L/W*. At constant *L/D* and *L/W*, the results show an opposite trend. The amplitude of surface pressure fluctuation decreases at larger *L/D*. The parameter *L/W* mainly affects the peak surface pressure fluctuation ahead of the rear face.

Nomenclature

C_p = static pressure coefficient, $(p_w - p_\infty)/q_\infty$
C_{σ_p} = pressure fluctuation coefficient, $(\sigma_p - \sigma_{p,\infty})/q_\infty$
D = cavity depth
L = cavity length
M = Mach number
p_w = wall pressure
q_∞ = freestream dynamic pressure
Re = unit Reynolds number
W = cavity width
x = streamwise distance
δ_0 = incoming boundary-layer thickness
σ_p = standard deviation of mean pressure

Introduction

CAVITIES occur in a large number of flight vehicles, projectiles, or engineering applications (such as a slotted-wall wind tunnel or gasdynamic laser cavity). They have been studied extensively in the past.[1–3] In general, introducing a cavity in a surface bounding flow changes the mean pressure distribution inside the cavity and in its vicinity. Drag of the aerodynamic component can be altered. Under certain conditions, high-intensity pressure fluctuations inside the cavity are produced due to the self-sustaining oscillation, which could excite vibration of the local structure and cause the damage of sensitive instrumentation. In addition, cavity flow contains a mixture of unsteady flow regimes that may include continuous shedding of vortices from the leading edge, pressure waves inside the cavity, and a large trailing-edge vortex oriented in the transverse direction.[4,5] Flow pattern is affected by the cavity geometry, Mach number, Reynolds number, and the state of incoming boundary layer. Furthermore, the cavity flowfield can be classified as open, transitional, or closed cavity flow. The type of flowfield appears to be a function of length-to-depth ratio L/D (Ref. 6). For an open cavity flow ($L/D < 10$), the high pressure ahead of the rear face venting into the low-pressure region downstream of the front face causes the shear layer to flow over or bridge the cavity. A study by Kim and Chokani[7] indicated that the shear layer is highly unsteady and constantly changes its shape and impingement location during the oscillation. Stronger and more coherent acoustic disturbances than that of the shear layer attachment at the cavity floor (closed cavity flow) are generated near the cavity trailing edge. Relatively uniform pressure over the cavity floor is slightly positive, and a small adverse pressure gradient occurs near the rear face due to the shear layer impingement. A transitional cavity flow, $(L/D)_{cr} = 10$–13, separates between open and closed cavity flows. The impingement shock and exit shock may be collapsing into a single wave. Mean surface pressure increases uniformly from a low value aft the front face to a peak value ahead of rear face. For $L/D > 13$, it is referred as closed cavity flow. The shear layer expands over the cavity leading edge, impinges on the cavity floor, and separates ahead of the rear face. This leads to two recirculation zones. Typical pressure distribution consists of a low-expansion region behind the front face, an increase due to the shear layer impingement, a pressure plateau in the impingement region, and a maximum ahead of the rear face. A study by Baysal and Stallings[8] shows that larger pressure is detected on the cavity rear face and smaller pressure is detected on the cavity front face than that of open cavity flow. This indicates higher drag for a closed cavity flow.

The length-to-width ratio L/W is generally referred as the three-dimensional parameter of a cavity flow.[9] The three-dimensional effect ($L/W > 1$) is in the form of larger lateral pressure gradient near the cavity rear face. At a higher value of L/W, shear layer instability is not being excited coherently along the span of the cavity and $(L/D)_{cr}$ decreases. This three-dimensional effect on the cavity pressure distribution is much greater for closed or transitional cavity flows than for open cavity flow.[6] Furthermore, the ratio of D/δ_0 is another dominant factor affecting the characteristics of a cavity flow. A decrease in D/δ_0 results in decreasing peak pressure values on both the cavity floor and rear wall,[6] which is considered to be due to less momentum carried by the shear layer and less energy transferred into the cavity from shedding vortices and impingement flow.

In addition, high-intensity pressure oscillation in a cavity flow is critical to the acoustic fatigue for an aerodynamic component. The pressure fluctuations consist mainly of discrete resonance. The frequency, amplitude, and harmonic property depend on the cavity geometry and external flow conditions. Tracy and Plentovich[10] indicated that the induced pressure fluctuation is due to a reinforcement between instabilities in the shear layer that bridges the cavity and pressure waves generated in the cavity when the shear layer impinges on the rear face. The dominating mechanisms include shear layer impingement, flow recompression, and trailing-edge vortex. These are strongly linked and form an oscillation cycle.[5] In other words, the shear layer impingement, formation of shock wave near the rear face, and mass removal/addition to the cavity dominate the oscillation environment and amplitude of pressure fluctuations.

Previous studies have mainly focused their effort on two-dimensional cavity flows, particularly for predicting the cavity modal frequencies of the oscillation.[11,12] The effect of L/W and D/δ_0 on mean and fluctuating pressure inside a cavity and in its vicinity needs to be further understood. More experimental data are

Received 5 August 1999; revision received 18 December 1999; accepted for publication 3 January 2000.

*Associate Research Fellow, Aerospace Science and Technology Research Center. Senior Member AIAA.

required. Thus, the purpose of this paper is to study the characteristics of transonic rectangular cavity flow at combination of L/D, L/W, and D/δ_0. Measurements of mean and fluctuating pressure are performed and analyzed.

Experimental Technique

Experiments are performed at the Aerospace Science and Technology Research Center/National Cheng-Kung University (ASTRC/NCKU) transonic wind tunnel. A boundary layer is developed naturally over a flat plate ahead of a rectangular cavity. Mean and fluctuating pressures are obtained at the plate surface ahead of the cavity ($x/L < 0$), the cavity floor ($0 < x/L < 1$), and the plate surface downstream of the cavity ($x/L > 1$). The following is a brief description of the facility, instrumentation, models, and test conditions.

Transonic Wind Tunnel

The ASTRC/NCKU transonic wind tunnel is a blowdown-type wind tunnel. The testing Mach number ranges from 0.2 to 1.4. Major components of the facility include compressors, air dryers, cooling water system, storage tanks, and the tunnel. The dew point of high-pressure air through the dryers is maintained at $-40°C$ under normal operating conditions. For the tunnel, a rotary perforated sleeve valve monitors the setup of stagnation pressure p_0. High-pressure air is discharged into the stilling chamber through flow spreaders. Inside the stilling chamber, there are acoustic baffles, screens, and a honeycomb to absorb control valve noise and to reduce freestream turbulence intensity. The test section, with solid side wall and perforated top/bottom walls in the present study, is 600×600 mm and 1500 mm in length. Downstream of the test section, a model support strut is installed for a sting-mounted pitot probe survey.

Data Acquisition Systems

An NEFF 620 data acquisition system and LeCroy (model 6810) waveform recorders are available for the experiments. The test conditions are recorded by the NEFF system, and a host computer (DEC Microvax 3500 minicomputer) controls the setup of NEFF system through high-speed interfaces. For surface pressure measurements, all pressure transducers are powered by a TES (model TES-6102) power supply at 15.0 V. A Twinhead 486 computer with CATALYST software controls the setup of LeCroy waveform recorders through a LeCroy 8901A interface. The typical sampling period in the present study is 5 μs. Also, external amplifiers (Ecreon Model E713) are used to improve the signal-to-noise ratio. With a gain of 20, the rolloff frequency is about 140 kHz.

Each data record possesses 131,072 data points for statistical analysis. The data are divided into 32 blocks. Mean and standard deviation (or fluctuating) values of each block (4096 data points) are calculated. Variation of the blocks is estimated to be 0.43 and 0.13% for C_p and C_{σ_p} values, respectively, which are considered the uncertainty of experimental data.

Testing Models and Instrumentation

The test model (Fig. 1) consists of a flat plate and an interchangeable instrumentation plate with a rectangular cavity. The test model is 150 mm wide and 600 mm long with a single-foot support mounted on the bottom wall of the test section. The front face of the cavity is located at 500 mm from the leading edge of the flat plate. For the surface pressure measurements, 22 instrumentation plates (150×150 mm) are fabricated. Length-to-depth ratio L/D ranges from 2.43 to 43.00, and the length-to-width ratio L/W is 0.5, 1.0, or 2.0. Depth-to-incoming boundary-layer thickness ratio D/δ_0 varies from 0.143 to 1.429. Furthermore, one row of 21 pressure taps along the centerline of each instrumentation plate is drilled perpendicularly to the test surface. All pressure taps are 6.0 mm apart and 2.5 mm in diameter. Because of the limit depth of the cavities, no pressure taps are available in the front or rear faces.

For an incoming boundary-layer survey, a Kulite pressure transducer (Model XCS-093-25A, B screen) is snuggled inside the pitot probe. The pressure transducer is located at 20 mm from the tip of the probe to ensure a fast response. The flattened intake is 2.0 mm wide and 0.3 mm high to minimize the displacement effects. A one-dimensional traversing mechanism is installed to move the pitot probe vertically to build a fairly detailed incoming boundary-layer profile. For surface pressure measurements, the same type of Kulite pressure transducer is used. The outside diameter of the pressure transducer is 2.36 mm, and the pressure sensitive sensor is 0.97 mm in diameter. Natural frequency of the transducers is 200 kHz as quoted by the manufacturer. Because the static calibration of a fast-response pressure transducer differs only by a few percent from the dynamic calibration,[13] the pressure transducers are calibrated statically only in the present study. Furthermore, the pressure transducers are flush mounted and potted using silicone rubber sealant. Resolution of surface pressure fluctuation is limited by the finite size of pressure transducer, that is, there is high-frequency damping due to the pressure transducer size. According to Corcos's criterion,[14] the maximum measurable frequency under the present test conditions is about 63 kHz, assuming the convection velocity $U_c = 0.65U_\infty$. However, Perng[2] indicated that the perforated screen of the Kulite pressure transducer may limit the frequency response only up to 50 kHz.

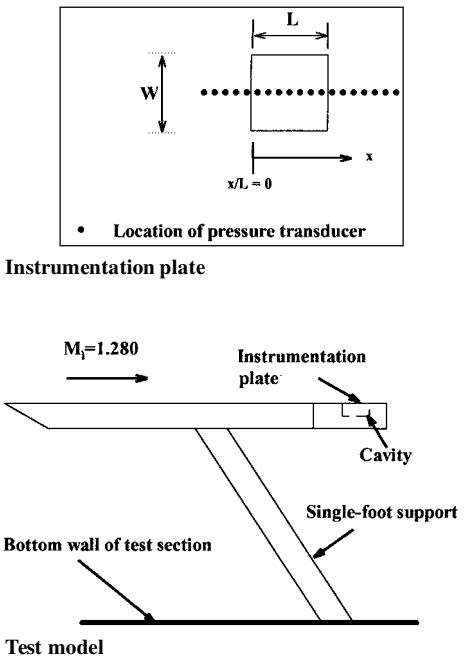

Fig. 1 Test configuration.

Test Conditions

In the present experiments, stagnation pressure and temperature are 193 ± 0.7 kPa and room temperature, respectively. Testing Mach number is 1.28 ± 0.01, and Re_{δ_0} (Reynolds number based on incoming boundary-layer thickness) is 2.1×10^5. An undisturbed boundary-layer survey conducted at 485 mm from the leading edge of the flat plate (or 15 mm ahead of cavity front face) shows that the normalized velocity profile appears to be full ($n \approx 9$ for velocity power law). This indicates a turbulent flow at the measurement locations, and the incoming boundary-layer thickness is 7.0 ± 0.2 mm.

Results and Discussion

Static Pressure Distributions

Mean surface pressure distributions for open ($L/D = 4.43$, 6.14, and 8.60), transitional ($L/D = 12.29$), and closed cavity flows ($L/D = 21.50$) are shown in Figs. 2–4. The data are presented in the form of pressure coefficients C_p, and the L/W effect on the static pressure is also illustrated. For open cavity flow (Fig. 2) the static pressure distributions show a slight upstream influence, gradual decrease in the first half of the cavity followed by a rise downstream (a concave curvature), a peak static pressure ahead of the rear face,

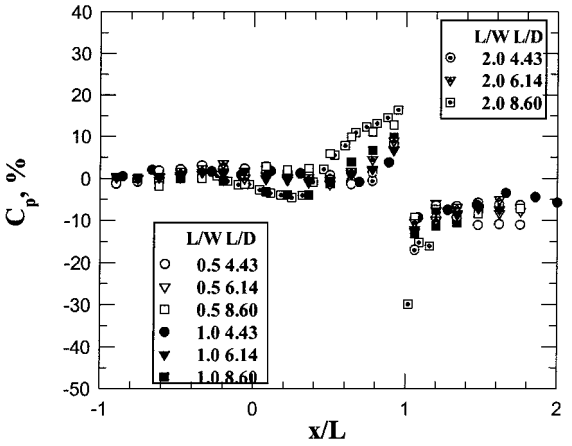

Fig. 2 Static pressure distributions: open cavity flow.

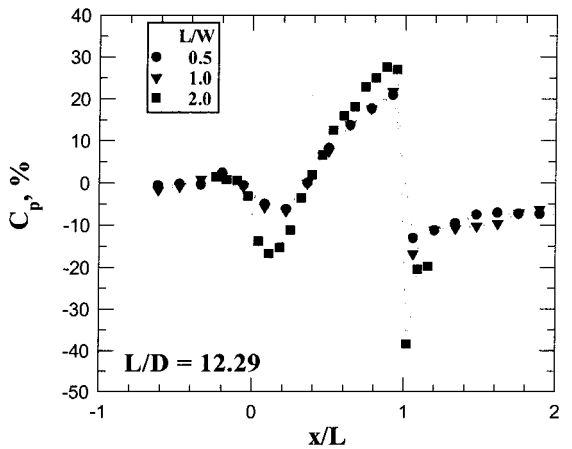

Fig. 3 Static pressure distributions: transitional cavity flow.

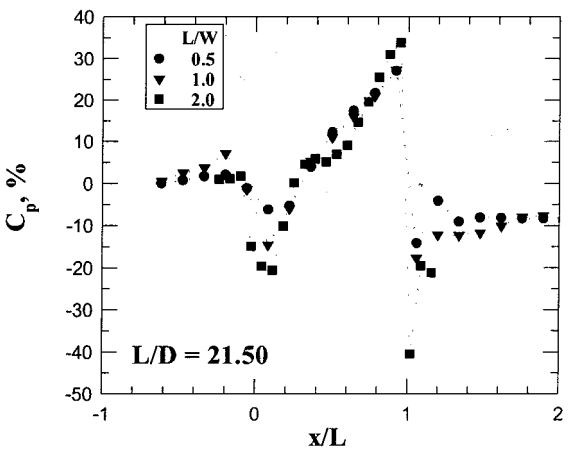

Fig. 4 Static pressure distributions: closed cavity flow.

large pressure variation over the cavity trailing edge, and new downstream equilibrium condition at about $x/L = 1.2$. In Stallings and Wilcox's measurements ($D/\delta_0 > 10$) (Ref. 6) the static pressure is relatively uniform in the cavity floor except for a spike ahead of the rear face ($x/L \approx 0.8$), which implies no vortex structure. In the present study, this concave curvature on the cavity floor is more evident as L/D increases at a given L/W, particularly for $L/D = 8.60$ at $L/W = 1.0$ and 2.0. Previous studies by Zhang and Edwards[5] and Perng[2] also show similar results. Zhang and Edwards indicated that this concave curvature is due to the shear layer diffusion in the first half of the cavity and large shear layer downward deflection near the trailing edge, in which shear layer diffusion results in gradually decreasing pressure and shear layer deflection causes a recompression (or pressure rise).[5] Perng further indicated that the ratio of D/δ_0 might be the possible reason for this concave curvature on the cavity floor.[2] The D/δ_0 for the present test cases ranges from 0.714 to 1.429, which is close to the tests of Zhang and Edwards[5] ($D/\delta_0 \approx 2.5$) and Perng[2] ($D/\delta_0 = 1.32$). It is possible that there might be some critical D/δ_0 on the open cavity flow. Further study is required. Moreover, it is observed that the peak pressure ahead of the rear face and pressure variation over the trailing edge increase with L/D, particularly for $L/W = 2.0$. This indicates that the three-dimensional effect is more significant in the rear part and immediately downstream of the cavity than that in the forward part of the cavity. For transitional cavity flow, the static pressure distributions (Fig. 3) show stronger expansion over the leading edge followed by a uniform increase toward the rear face. Peak pressure ahead of the rear face and pressure variation over the trailing edge are more pronounced compared with that of open cavity flow, particularly for $L/W = 2.0$. As L/D is further increased, the static pressure distributions show a trend similar to that of transitional cavity flow. However, the static pressure distributions show better agreement for all three test cases. This indicates that the three-dimensional effect is minimized for closed cavity flow (Fig. 4).

Variations of the static pressure at five locations (plate surface upstream of the cavity, downstream of the front face, middle, ahead of the rear face, and plate surface downstream of the cavity) at a given L/W are summarized in Figs. 5–7. The effect of L/D on the static pressure is also illustrated. The static pressure appears to be highest ahead of the rear face and lowest at the immediate plate surface downstream of the cavity. For the open cavity flows ($L/D < 8.60$), the static pressure at the center and near the front face is roughly the same. As L/D increases, the static pressure at

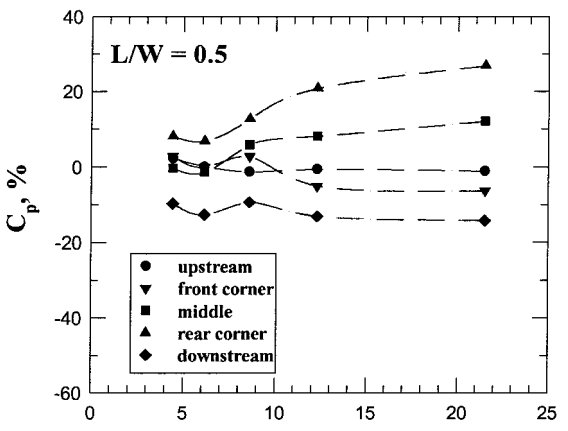

Fig. 5 Static pressure at $L/W = 0.5$.

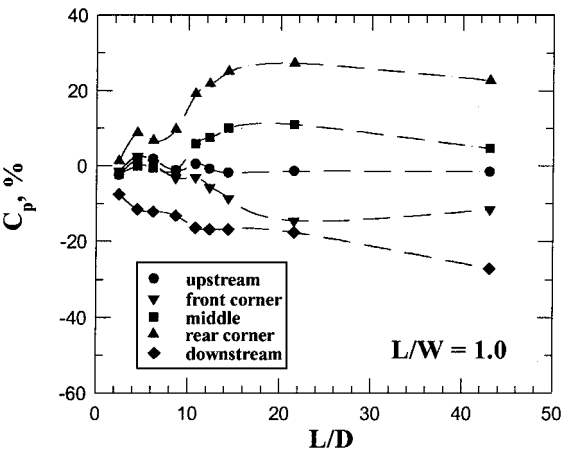

Fig. 6 Static pressure at $L/W = 1.0$.

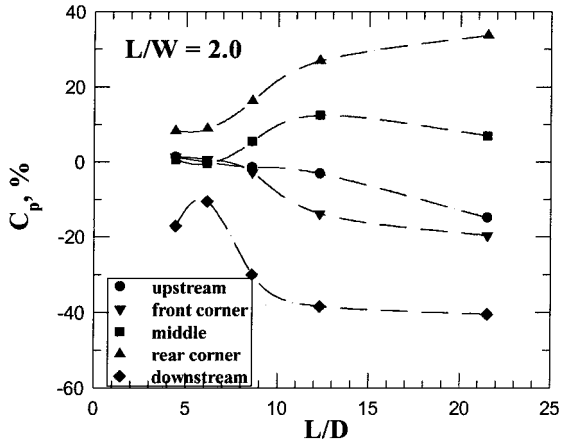

Fig. 7 Static pressure at $L/W = 2.0$.

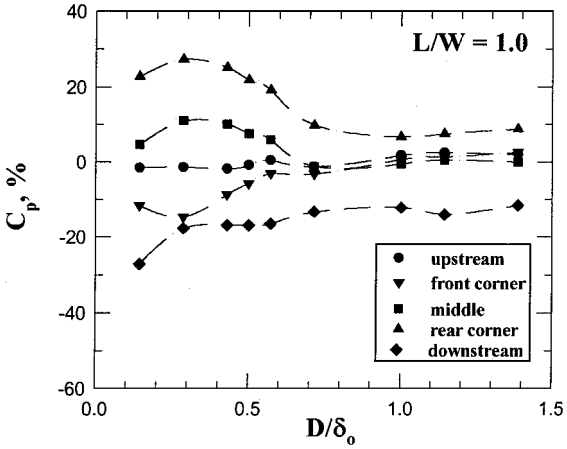

Fig. 9 Static pressure: D/δ_0 effect.

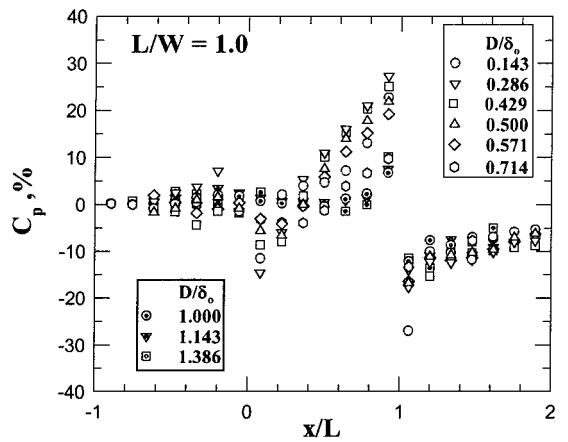

Fig. 8 Static pressure distributions: D/δ_0 effect.

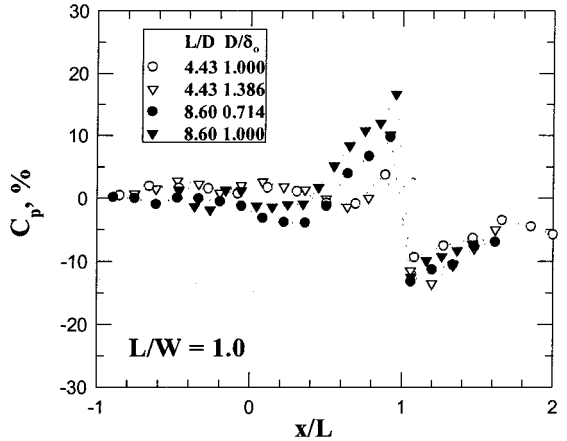

Fig. 10 Static pressure distributions: D/δ_0 effect at given L/D and L/W.

the center is higher than that near the front face. In addition, the data of all of the test cases also display a similar L/D trend. Variations of the static pressure show transitional behavior at $L/D = 6.14$–12.25, which should correspond to a switching of the type of cavity flowfield. For $L/D > 12.50$ (transitional and closed cavity flows), smaller static pressures are detected aft of the front face, and larger static pressures are detected ahead of the rear face than those of open cavity flow. Also note that the three-dimensional effect ($L/W = 2.0$) is more significant on the static pressures ahead of the rear face and the plate surface downstream of the cavity. This is similar to the computational result of Suhs,[15] in which the presence of a fully developed vortical structure in the aft half of the cavity results in higher pressure level for a three-dimensional flowfield.

Furthermore, the static pressure distributions are replotted at different D/δ_0 (Fig. 8). The cavity length and width are held constant ($L/W = 1.0$) as depth varies. Thus, the scaling parameter D/δ_0 changes as D varies. For $D/\delta_0 \leq 0.571$, the data again represent transitional and closed cavity flows. There is lack of agreement among the data, particularly near the front and rear face on the cavity floor. For $D/\delta_0 \geq 0.714$ (or open cavity flow), the data show much better correlation on the upstream plate surface, floor, and downstream plate surface of the cavities. The static pressures at five locations are further summarized to illustrate the effect of D/δ_0 on the characteristics of cavity flows (Fig. 9). The data indicate that static pressures at all locations are nearly constant for $D/\delta_0 \geq 0.714$. The static pressures at the upstream plate surface and the front-half of the cavity floor (downstream of the front face and the middle locations) are roughly the same. With decreasing D/δ_0, higher static pressure at the aft half of cavity floor (middle and ahead of the rear face) and lower static pressures near the front face are obtained. The results do not agree with the study of Stallings and Wilcox[6] at different depths but constant values of L/D and L/W. Thus, further experiments are conducted for the tests of D/δ_0 effect at constant L/D and L/W (Fig. 10). At $L/D = 4.43$, the effect of D/δ_0 is not significant, except for the spike ahead of the rear face. The static pressure ahead of the rear face for $D/\delta_0 = 1.386$ is higher than that for $D/\delta_0 = 1.000$. At $L/D = 8.60$, the pressure levels at the plate surface upstream and downstream of the cavities are roughly the same, but there is some disagreement on the floor, in which higher levels of surface pressure are observed with increasing D/δ_0. This shows an opposite trend only when L/W is held constant.

Pressure Fluctuations

Measurements of fluctuating pressure on the floor and in the vicinity of the cavities are conducted to understand the effect of cavity geometry on the amplitude of surface pressure fluctuations. Distributions of normalized pressure fluctuation C_{σ_p} are shown in Figs. 11–13. C_{σ_p} represents the relative amplitude of local pressure fluctuation $\sigma_{p,w}$ with respect to the freestream condition $\sigma_{p,\infty}$. For open cavity flows, the distributions of C_{σ_p} (Fig. 11) show a similar trend. The levels of fluctuating pressure increase slightly at the plate surface upstream of the cavity, which corresponds to the upstream propagation of the disturbance created by the presence of the cavity. Expansion over the cavity leading edge causes the damping downstream of the front face, followed by a gradual increase to a minor peak at about the middle of the floor. Peak surface pressure fluctuations ahead of the rear face are considered to be due to the recompression, trailing-edge vortex, and high-energy inflow. At a plate surface downstream of the cavity, C_{σ_p} decreases and approaches new equilibrium levels at $x/L \approx 1.2$–1.4. This may represent the downstream influence region of the cavity. Also note that the variations of L/W and L/D do not significantly affect the levels of C_{σ_p} for all of the test cases, an exception being the peak surface pressure fluctuation $C_{\sigma_p,\max}$ ahead of the rear face. $C_{\sigma_p,\max}$

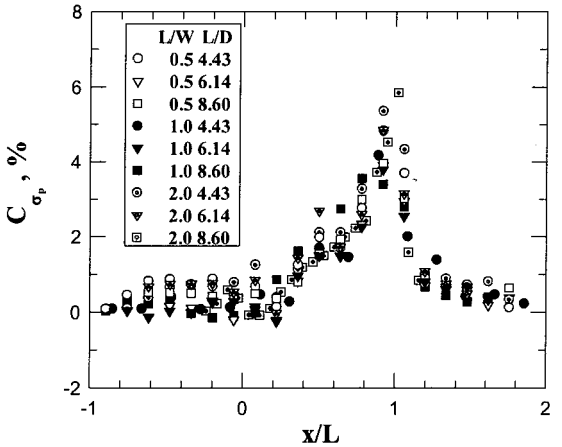

Fig. 11 Surface pressure fluctuation: open cavity flow.

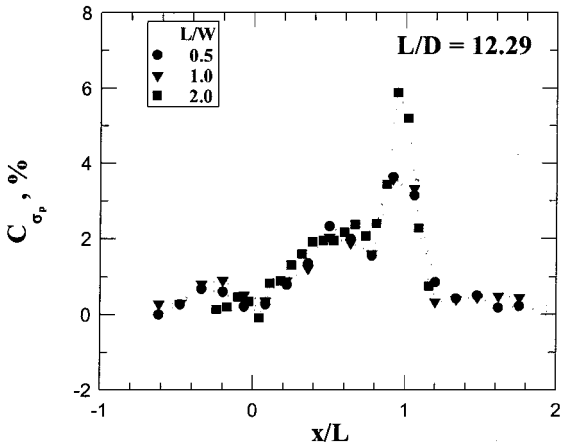

Fig. 12 Surface pressure fluctuation: transitional cavity flow.

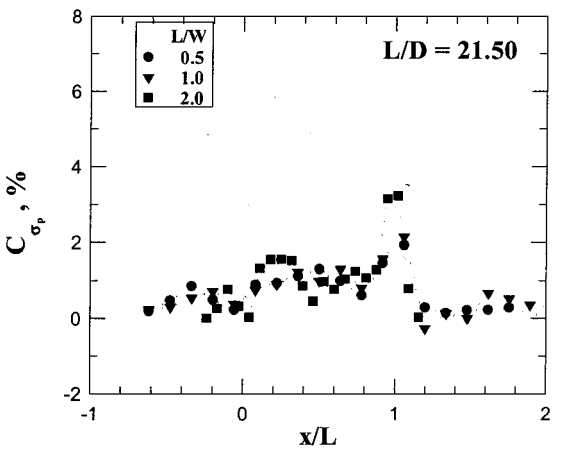

Fig. 13 Surface pressure fluctuation: closed cavity flow.

decreases slightly with increasing L/D. At $L/W = 2.0$, $C_{\sigma_p,\max}$ is about 1–2% higher than that at $L/W = 0.5$ and 1.0. For transitional cavity flows ($L/D = 12.29$, Fig. 12), the distributions of C_{σ_p} for three test cases show good agreement. The trend of the variation of C_{σ_p} is similar to that of open cavity flows. The parameter L/W only affects the peak surface pressure fluctuation ahead of the rear face. As L/D further increases (closed cavity flows, Fig. 13), the level of surface pressure fluctuation is considerably lower than that of open and transitional cavity flows. This agrees with the results of Zhang and Edwards,[5] in which attenuation of the surface pressure fluctuation with increasing L/D corresponds to the upward movement of the trailing-edge vortex and subsequent reduction of high-energy

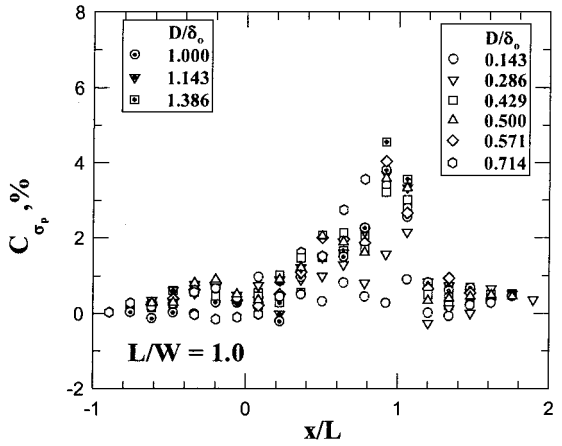

Fig. 14 Surface pressure fluctuation: D/δ_0 effect.

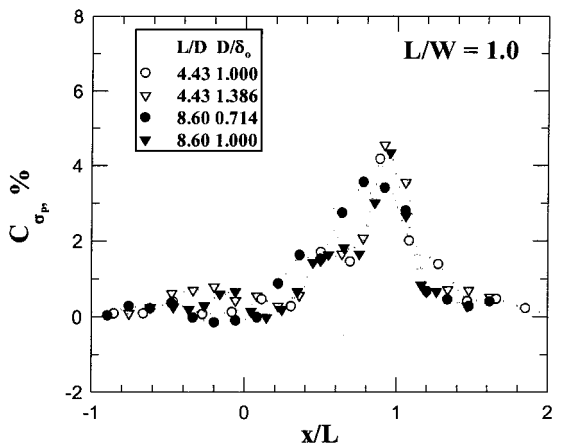

Fig. 15 Surface pressure fluctuation: D/δ_0 effect at given L/D and L/W.

flow into the cavity. It is also observed that the three-dimensional effect is minimized for the closed cavity flow. At $L/W = 2.0$, $C_{\sigma_p,\max}$ is only up to 1% higher than that at $L/W = 0.5$ and 1.0. This indicates that the three-dimensional effect is more significant for open and transitional cavity flows.

The data of surface pressure fluctuation are replotted with different D/δ_0 for $L/W = 1.0$ (Fig. 14). In general, the levels of C_{σ_p} in the upstream plate surface, cavity floor, and downstream plate surface increase with D/δ_0. This again indicates higher levels of surface pressure fluctuation for open and transitional cavity flows. Particularly, the peak surface pressure fluctuations ahead of the rear face increase significantly at higher D/δ_0, up to 3% of dynamic pressure q_∞. A study by Perng[2] indicates the presence of a small corner vortex for the open cavity flows. This corner vortex causes a high level of surface pressure fluctuation ahead of and on the rear face. Thus, the present data may imply a diminishing corner vortex at smaller D/δ_0 (or closed cavity flows). Furthermore, the D/δ_0 effect at given L/D and L/W on surface pressure fluctuation is shown in Fig. 15. At $L/D = 4.43$, the distributions of surface pressure fluctuation for $D/\delta_0 = 1.000$ and 1.386 show good agreement except at the upstream plate surface. This indicates further upstream propagation of a disturbance at larger D/δ_0, which is also evident for test cases of $L/D = 8.60$. In addition, the data along the rear part on the cavity floor for $L/D = 8.60$ show a lack of agreement. This could be due to the influence of the trailing-edge vortex.[2]

Conclusions

The present investigation examines the effects of variation of the length-to-depth L/D, length-to-width ratio L/W, and depth-to-incoming boundary-layer thickness D/δ_0 on the characteristics of

low-supersonic rectangular cavity flow. The results of this study are summarized as follows:

1) The static pressure distributions for open cavity flow show a concave curvature on the cavity floor. This concave curvature is more pronounced with increasing L/D.

2) For transitional and closed cavity flows, there is stronger expansion over the leading edge and larger pressure variation near the rear face compared with those of open cavity flow.

3) A higher pressure level in the aft part of the cavity is obtained for a three-dimensional flowfield, and the three-dimensional effect is minimized for closed cavity flow.

4) At constant L/W, decreasing cavity depth results in lower static pressure aft of the front face and higher static pressure in the aft part of the cavity. This shows the opposite trend when both L/W and L/D are held constant.

5) The levels of surface pressure fluctuation in the cavity floor and its vicinity decrease with increasing L/D. Variation of L/W mainly affects the peak surface pressure fluctuation ahead of the rear face, up to 1–2% of dynamic pressure. This three-dimensional effect is more significant for open and transitional cavity flows.

6) There is further upstream propagation of disturbances at larger D/δ_0 at given L/D and L/W.

Acknowledgments

The National Science Council sponsored this research (NSC 88-2612-E-006-004). The support is gratefully acknowledged. The author also thanks the technical support of the Aerospace Science and Technology Research Center/National Cheng-Kung University technical staffs with the experiments.

References

[1]Komerath, N. M., Ahuja, K. K., and Chambers, F. W., "Prediction and Measurement of Flows over Cavities: A Survey," AIAA Paper 87-0166, Jan. 1987.

[2]Perng, S., "Passive Control of Pressure Oscillations in Hypersonic Cavity Flow," Ph.D. Dissertation, Aerospace Engineering Dept., Univ. of Texas, Austin, TX, Dec. 1996.

[3]Rockwell, D., and Naudascher, E., "Review–Self Sustaining Oscillations of Flow Past Cavities," *Journal of Fluids Engineering*, Vol. 100, No. 2, 1978, pp. 152–165.

[4]Disismile, P. J., and Orkwis, P. D., "Effect of Yaw of Pressure Oscillation Frequency with Rectangular Cavity at Mach 2," *AIAA Journal*, Vol. 35, No. 7, 1997, pp. 1323–1325.

[5]Zhang, X., and Edwards, J. A., "An Investigation of Supersonic Cavity Flows Driven by Thick Shear Layers," *Aeronautical Journal*, Vol. 94, No. 940, 1990, pp. 355–364.

[6]Stallings, R. L., Jr., and Wilcox, F. J., Jr., "Experimental Cavity Pressure Distributions at Supersonic Speeds," NASA TP-2683, June 1987.

[7]Kim, I., and Chokani, N., "Navier–Stokes Study of Supersonic Cavity Flowfield with Passive Control," *Journal of Aircraft*, Vol. 29, No. 2, 1992, pp. 217–223.

[8]Baysal, O., and Stallings, R. L., Jr., "Computational and Experimental Investigation of Cavity Flowfields," *AIAA Journal*, Vol. 26, No. 1, 1988, pp. 6, 7.

[9]Ahuja, K. K., and Mendoza, J., "Effects of Cavity Dimensions, Boundary Layer, and Temperature on Cavity Noise with Emphasis on Benchmark Data to Validate Computational Aeroacoustic Codes," NASA CR-4653, April 1995.

[10]Tracy, M. B., and Plentovich, E. B., "Measurements of Fluctuating Pressure in a Rectangular Cavity in Transonic Flow at High Reynolds Numbers," NASA TM-4363, June 1992.

[11]Bilanin, A. J., and Cover, E. E., "Estimation of Possible Excitation Frequencies for Shallow Rectangular Cavities," *AIAA Journal*, Vol. 11, No. 3, 1973, pp. 347–351.

[12]Rockwell, D., "Prediction of Oscillation Frequencies for Unstable Flow Past Cavities," *Journal of Fluids Engineering*, Vol. 99, No. 2, 1977, pp. 294–300.

[13]Chung, K. M., and Lu, F. K., "Shock Tube Calibration of a Fast-Response Pressure Transducer," AIAA Paper 90-1399, June 1990.

[14]Corcos, G. M., "Resolution of Pressure in Turbulence," *Journal of the Acoustical Society of America*, Vol. 35, No. 2, 1963, pp. 192–199.

[15]Suhs, N. E., "Computation of Three-Dimensional Cavity Flow at Subsonic and Supersonic Mach Numbers," AIAA Paper 87-1208, June 1987.